Title

Integrating phase and composition of secondary organic aerosol from the ozonolysis of α-pinene.

Journal

Proceedings of the National Academy of Sciences of the United States of America, 111(21)

ISSN

1091-6490

Authors

Kidd, Carla
Perraud, Véronique
Wingen, Lisa M
et al.

Publication Date

2014-05-27

Peer reviewed

Integrating phase and composition of secondary organic aerosol from the ozonolysis of α-pinene

Carla Kidd, Véronique Perraud, Lisa M. Wingen, and Barbara J. Finlayson-Pitts[1]

Department of Chemistry, University of California, Irvine, CA 92697

Edited* by Mark H. Thiemens, University of California, San Diego, La Jolla, CA, and approved April 16, 2014 (received for review December 3, 2013)

Airborne particles are important for public health, visibility, and climate. Predicting their concentrations, effects, and responses to control strategies requires accurate models of their formation and growth in air. This is challenging, as a large fraction is formed by complex reactions of volatile organic compounds, generating secondary organic aerosol (SOA), which grows to sizes important for visibility, climate, and deposition in the lung. Growth of SOA is particularly sensitive to the phase/viscosity of the particles and remains poorly understood. We report studies using a custom-designed impactor with a germanium crystal as the impaction surface to study SOA formed from the ozonolysis of α-pinene at relative humidities (RHs) up to 87% at 297 ± 2 K (which corresponds to a maximum RH of 70–86% inside the impactor). The impaction patterns provide insight into changes in phase/viscosity as a function of RH. Attenuated total reflectance-Fourier transform infrared spectroscopy and aerosol mass spectrometry provide simultaneous information on composition changes with RH. The results show that as the RH at which the SOA is formed increases, there is a decrease in viscosity, accompanied by an increasing contribution from carboxylic acids and a decreasing contribution from higher molecular mass products. In contrast, SOA that is formed dry and subsequently humidified remains solid to high RH. The results of these studies have significant implications for modeling the growth, aging, and ultimately, lifetime of SOA in the atmosphere.

aerosol phase | SOA viscosity | oligomers | SOA composition | particle bounce

Airborne particles negatively affect health (1) and visibility (2–4), and their effects on climate are substantial (2, 3, 5–7). A large portion of atmospheric particulate matter comprises low-volatility organics formed during gas phase oxidation of hydrocarbons, including biogenics. This organic contribution, which is typically more than 50% of the total particle mass (8–10), is often underpredicted by models. Although recent measurement-model comparisons are in closer agreement (11–15), challenges remain because of the complexity of SOA. For example, despite improvements in modeled mass loading, there remain issues when trying to predict specific characteristics such as oxygen-to-carbon ratio and volatility (16) simultaneously.

It is vital that models and measurements are in agreement for the right reasons to have robust predictive capability. A potential contributor to the remaining discrepancies could be the assumptions incorporated into the models. Specifically, SOA has been generally considered to be a low-viscosity liquid that equilibrates with the surrounding gases, with no condensed phase diffusion limitations on the scale of the time steps used in the models (17, 18). However, there is recent evidence for solid or semisolid phases of SOA, such as much slower evaporation than expected (19, 20), SOA composition that is consistent with irreversible condensational growth (21), viscosity measurements (22), time for mixing and uptake of reactive gases such as NH_3 (23, 24), behavior on heating (25), and bounce of SOA from impactor surfaces (26–29). The use of bounce as an indicator of phase is based on the assumption that solids or semisolids striking the surface can bounce, whereas liquids will not. Many of these studies were carried out on SOA at low (<5%) relative humidity (RH) (19–21, 23–25), and in studies of RH effects on phase or viscosity, the SOA was formed under relatively dry conditions and subsequently humidified (22, 28).

Solid and semisolid particles will exhibit very different behavior than liquid particles (30–33). For example, instead of instantaneous gas-particle partitioning of semivolatile compounds, irreversible condensation will be a more accurate description for particle growth. Incorporating a condensation mechanism into a model for SOA particle growth has been shown to reproduce field data better than using equilibrium partitioning alone (34). Including measured physical properties of SOA, such as the diffusion coefficient, has also recently been shown to aid accurate prediction of SOA mass (35).

In the present studies, data relevant to the viscosity and composition of SOA formed during the ozonolysis of α-pinene at a range of RH are obtained simultaneously. A custom-designed impactor is used to collect SOA onto an infrared-transmitting attenuated total reflectance (ATR) crystal for analysis by infrared (IR) spectroscopy, accompanied by supporting aerosol mass spectrometry (AMS) measurements of the SOA. The impaction patterns on the crystal reveal changes in particle phase and viscosity as the RH during the formation of SOA is varied, and the IR and MS data provide information on changes in composition. This combination of approaches provides unique insight into the relationship between physical properties (phase/viscosity) and molecular composition and their dependence on RH. To isolate the effects of RH alone on the impaction patterns, experiments are also carried out using SOA formed dry and subsequently humidified.

Results and Discussion

Particle Impaction Patterns. Particles were collected on a germanium (Ge) ATR crystal, using the custom-designed impactor described in detail in *SI Appendix, Impactor Characterization* (*SI Appendix*, Fig. S1). The particle-laden air is pumped at a flow

Significance

The phase of atmospheric aerosol particles can have dramatic effects on reactivity, growth, oxidation, and water uptake. As such, it plays a critical role in every aspect of particle evolution. Despite this, our knowledge of the phase of secondary organic aerosol (SOA) and how it changes in relation to conditions during SOA formation, particle history, composition, relative humidity, and temperature remains poor. Recent laboratory experiments suggest that SOA, under certain circumstances, is best described as a semisolid or viscous tar. This work shows how phase/viscosity, water availability during SOA formation, and composition are interrelated and offers mechanistic insights into these relationships.

Author contributions: C.K., V.P., L.M.W., and B.J.F.-P. designed research; C.K., V.P., and L.M.W. performed research; C.K., V.P., L.M.W., and B.J.F.-P. analyzed data; and C.K., V.P., L.M.W., and B.J.F.-P. wrote the paper.

The authors declare no conflict of interest.

*This Direct Submission article had a prearranged editor.

Freely available online through the PNAS open access option.

[1]To whom correspondence should be addressed. E-mail: bjfinlay@uci.edu.

This article contains supporting information online at www.pnas.org/lookup/suppl/doi:10.1073/pnas.1322558111/-/DCSupplemental.

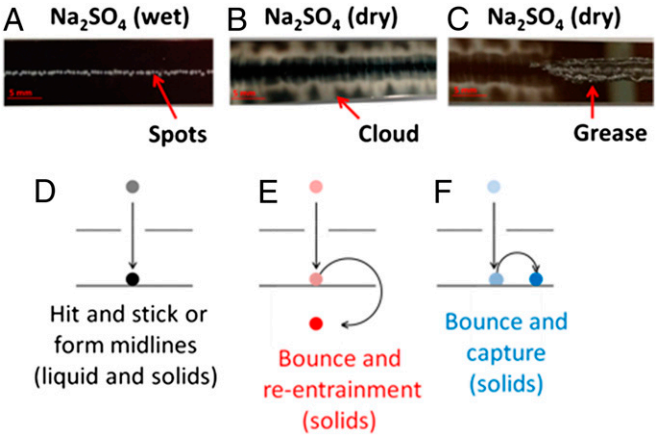

Fig. 1. Digital photographs of impacted wet (*A*) and dry (*B* and *C*) Na_2SO_4 particles. Particle bounce (identified as the cloud) is suppressed when the center of the crystal is coated with grease (*C*). Also shown (*D*–*F*) are schematic illustrations of the simplified mechanisms available to impacting particles. [Red scale bar (*A*–*C*): 5 mm.]

rate of 30 L·min^{-1} through the holes in the orifice plate. Particles above a certain size have sufficient momentum to impact on the ATR crystal, whereas smaller particles continue in the airstream and are pumped around the long edges of the crystal. Measurements of the collection efficiency for the impactor as a function of particle size using carboxylate-modified latex (CML) spheres (36) give a 50% cut-off diameter (d_{50}) of 240 ± 12 nm (*SI Appendix*, Fig. S2). The mass and number size distributions for dry SOA (<3% RH) are such that a significant fraction of the particles by number and most of the SOA mass will be collected by the impactor (*SI Appendix*, Fig. S2).

Particle bounce is a well-documented problem when collecting atmospheric particles by impaction (4, 37–41) and can also contribute to reduced collection efficiencies in aerosol mass spectrometers (42, 43). Recently, however, these bounce phenomena have been used to probe SOA phase in laboratory and field campaigns (26–28, 44). Particle numbers before and after the impactor gave the fraction of particles that bounced as a measure of nonliquid particles. SOA from α-pinene and longifolene showed relatively little change in the bounce fraction (~0.8), as the RH to which the preformed particles were subsequently exposed was increased up to an impactor RH of 65% (28), indicating the particles are solids or semisolids. In the present studies, we show that a particle that has initially bounced need not exit the impactor and that the impaction patterns thus formed can provide insight into particle phase/viscosity. The patterns made by impacting particles onto the Ge substrate were recorded by digital photography, optical microscopy, and scanning electron microscopy (SEM). Standards of known phase were generated and impacted as described in *SI Appendix, Generation and Impaction of Atomized Standards* and *SI Appendix, Size Distributions, Impaction Patterns and Microscope Images of Wet and Dry Na_2SO_4*.

Fig. 1 shows photographs for deliquesced (Fig. 1*A*) and dry (Fig. 1*B*) Na_2SO_4 particles. The impacted salt particles appear as a lighter color on the black Ge substrate. Optical microscope and SEM images showing magnified features are provided in *SI Appendix*, Figs. S3 and S4, and the size distributions are provided in *SI Appendix*, Fig. S5. Clearly, the wet and dry Na_2SO_4 cases generate very different impaction patterns. The liquid particles are collected as primary deposits and form a line of spots along the centerline, mirroring the pattern of the holes in the orifice plate above. From the SEM images (*SI Appendix*, Fig. S4), it can be seen that the spots are slightly larger than the orifice diameter (0.2 mm), as expected (45). For dry Na_2SO_4 (solid particles), no material collects in the center of the crystal where the particles initially impact. Instead, a cloud of material is observed extending out to the crystal edges, well away from the primary impaction point.

An impacting particle may hit and stick to the substrate immediately below the orifice, forming spots (Fig. 1*D*); may form midlines between the spots because of multiorifice interactions (45) of initially bounced particles; may bounce and be re-entrained in the gas stream to be pumped away (Fig. 1*E*); or may bounce on first impact but be subsequently captured on the substrate (Fig. 1*F*). Of these options, Fig. 1 *E* and *F* are only possible for particles that are not liquid. Although bounce and capture was previously postulated (46) for nonliquid particles, to the authors' knowledge, it has not been documented experimentally.

The patterns in Fig. 1 *A* and *B* show that wet Na_2SO_4 particles undergo a hit-and-stick mechanism, whereas dry Na_2SO_4 particles undergo bounce and capture to yield the cloud pattern. Confirming this interpretation is the impaction pattern for the dry salt when a thick layer of highly viscous vacuum grease was applied along half (right side) of the centerline of the crystal to prevent bounce (Fig. 1*C*): No cloud was seen where grease was applied, and spots in the grease can be seen corresponding to the orifice pattern, whereas on the ungreased portion, the cloud pattern remains.

When a particle approaches a surface, it experiences attractive adhesion (van der Waals) interactions with the surface. Liquid particles deform on impact and generally do not have sufficient rebound energy to escape. However, solid particles with sufficient energy will bounce (47). Larger, denser, and higher incident kinetic energy solid particles will suffer greater bounce and rebound with more energy (4, 47–50). Although bounce is diagnostic of solid particles, the lack of bounce cannot necessarily be used to identify liquid particles, as smaller solid particles having less momentum can also hit and stick.

The effect of particle size on the impaction patterns, independent of other factors, was investigated using solid CML spheres of known size and density (36). The original impaction point for both 270- and 600-nm CML spheres is directly beneath the orifices, with larger particles hitting closer to the midpoint of the orifice because of their larger momentum (4, 51). As can be seen in Fig. 2*A*, spots resulting from hit and stick are observed for 270-nm spheres, the size of which is close to the d_{50} of the impactor. In the case of 600-nm spheres (Fig. 2*B*), there is a cloud resulting from bounce and capture as well as a significant amount of material near the centerline; however, 600-nm CML spheres do not form spots at the original impaction site but, rather, at the midlines. In this case, flow stagnation resulting from interactions from adjacent orifices increases impaction (45). A recent study that used flow fields and particle trajectory calculations, along with experimental studies of the impaction patterns formed by supermicron liquid oleic acid particles in a dual orifice test impactor (45), showed similar spots and midline patterns. No cloud equivalent was observed, as expected for their liquid particles.

A size effect can also be seen with dry polydisperse caffeine particles (for size distribution, see *SI Appendix*, Fig. S6). Both spots and clouds are seen (Fig. 2*C*); thus, despite all of the particles in the polydisperse dry sample being solid and of the same density, some stick on first impact (forming spots), whereas others bounce (forming a cloud). The dictating factor for bounce in this case is

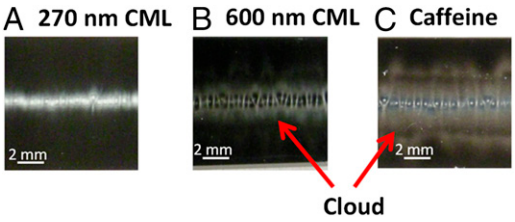

Fig. 2. Digital photographs of impaction patterns on a Ge ATR crystal substrate formed by impacting (*A*) 270-nm CML spheres (*B*) 600-nm CML spheres, and (*C*) polydisperse caffeine.

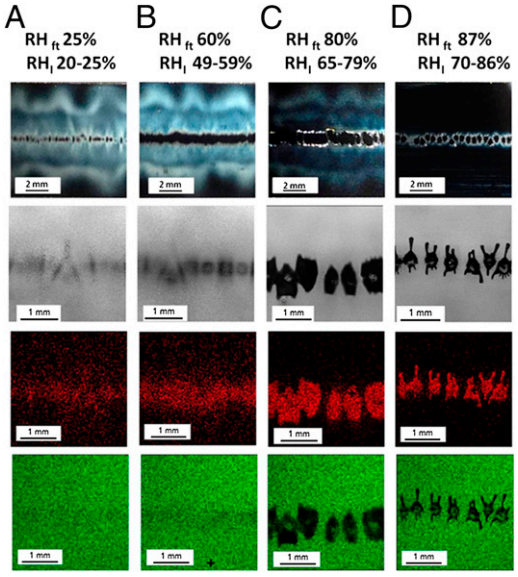

Fig. 3. Digital photographs (*First row*), SEM images (*Second row*) and energy dispersive spectroscopy elemental maps (*Third* and *Fourth rows*) of the impaction patterns of SOA on a Ge substrate. Elemental map is for carbon (red) and Ge (green). The SOA was generated at various RH_{ft} (from 25–87%, *A–D*) and subjected to the corresponding RH_I (20–86%, *A–D*) inside the impactor.

purely particle size, with larger particles rebounding with greater kinetic energy (47) to form the clouds and with smaller particles forming spots because of hit and stick. The cloud pattern observed in this study will likely be influenced by impactor design; a wide substrate, for example, may aid the collection of initially bounced particles. A faster flow rate may increase the prevalence of a cloud over spots, as bounce probability is related to impact speed, but investigation of such factors were beyond the scope of this study.

Impaction Patterns of SOA Formed at, and Humidified to, Various RH. Fig. 3 *A–D* shows the impaction patterns on the ATR crystal for SOA collected from the reaction of ozone (650 ppb) with α-pinene (800 ppb), generated at flow tube reaction RH (RH_{ft}) from 25–87% (21, 52). As a result of a pressure drop in the impactor (*SI Appendix, Influence of Impactor Pressure Drop Inside the Impactor*), the particles experience reduced RH just before impaction; both the flow tube RH as well as the calculated maximum and minimum RH inside the impactor are provided [RH_I(min–max)] in Fig. 3. As shown in *SI Appendix*, Fig. S7, the shapes of the size distributions are similar as the RH is increased, and thus the changes observed in Fig. 3 *A–D* reflect primarily changes in the physical properties of the particles and/or changes resulting from the presence of water inside the impactor.

The bounced SOA in the photographs (Fig. 3, *First row*) appears white because of light scattered and reflected from the impacted particles against the black background of the Ge crystal. The black strip along the centerline at increasing RH actually includes impacted SOA but appears black, as it becomes a non-light-scattering film rather than reflective particles. This was difficult to capture by photography but is evident in the SEM images and associated C and Ge elemental maps generated by energy dispersive spectroscopy (Fig. 3).

The impaction patterns for polydisperse SOA formed at low RH ($RH_{ft} \leq 25\%$) (Fig. 3*A*) are very similar to that from atomized caffeine particles (Fig. 2*C* and *SI Appendix*, Fig. S6), with spots, clouds, and midlines. This is consistent with SOA and caffeine having the same density (1.2 $g \cdot mL^{-1}$) (21) and similar size distributions above 200 nm (*SI Appendix*, Fig. S6). In the context of SOA phase, the impaction patterns clearly show that laboratory-generated SOA formed under dry conditions ($RH_{ft} \leq 25\%$) from the reaction between ozone and α-pinene forms solid particles that bounce on impact. Experiments were also performed at lower concentrations (300 ppb α-pinene, 200 ppb ozone) and in the presence of an OH scavenger; no differences in impaction patterns were observed. One caveat is that these are higher concentrations than typically encountered in the atmosphere. However, the results are consistent with a number of recent laboratory and field experiments that have found that SOA, at least at low RH, is best described as a semisolid or viscous tar (19–28, 32).

Surprisingly, the presence of a discernible cloud pattern up to 80% RH_{ft} (Fig. 3*C*; RH_I = 65–79%) shows that bounce and capture, and therefore nonliquid (solid or semisolid) particles, occur to some extent even for SOA formed at this high RH. At 87% RH_{ft} (RH_I = 70–86%), the particles are all collected along the center of the substrate and are therefore undergoing hit and stick (Fig. 3*D*). This trend suggests a decrease in viscosity of the particles with increasing RH_{ft} because of compositional changes and/or water uptake into the particles.

However, a potential contributor to the changes in the impaction patterns is the influence of water in the impactor (*SI Appendix, Effect of Varying RH_I on Impaction Patterns*). An increase in the collection efficiency (reduction of bounce) of ambient particles (33, 53, 54) and laboratory-generated aerosols (41, 55) as the RH increases has been attributed to adsorbed water on the particles and/or substrate, independent of phase. (Note that if humidity in the impactor were aiding the collection of particles, the SOA may be more solid than the patterns imply). Recent work by Bateman and coworkers (55) shows that for solid hydrophobic polystyrene spheres at diameters close to the d_{50}, there can be a significant decrease in bounce as RH in the impactor is increased. This effect is reduced as particle size increases, and for diameters greater than twice the d_{50}, all particles bounce regardless of RH. The mean diameter of the SOA in the present experiments (*SI Appendix*, Fig. S7) was over this threshold, so the dramatic changes observed from 80 to 90% RH are unexpected unless the particle viscosity also changes.

To separately determine the effect of RH on the impaction patterns in this system, a series of experiments was carried out using SOA that was formed under dry conditions ($RH_{ft} < 3\%$) and subsequently humidified by dilution in humid air to the final RH (RH_{entry}). These are designated "dry-wet" experiments. The

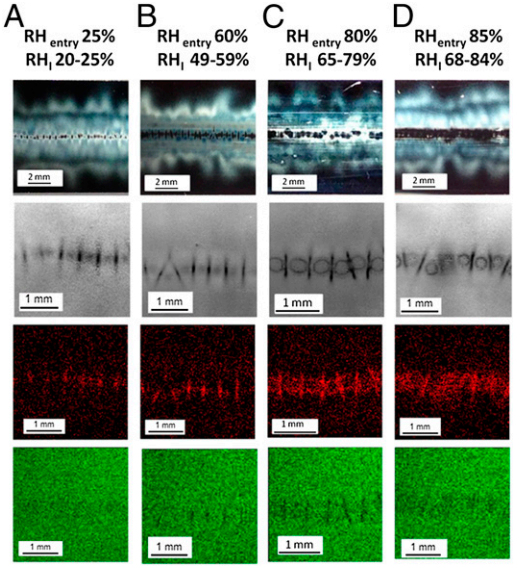

Fig. 4. Digital photographs (*First row*), SEM images (*Second row*), and energy dispersive spectroscopy elemental maps (*Third* and *Fourth rows*) of the impaction patterns of SOA formed under dry conditions and then humidified ("dry-wet"). The SOA was humidified to various RH_{ft} (from 25–85%, *A–D*) and subjected to the the corresponding RH_I (20–84%, *A–D*) inside the impactor. Elemental map is for carbon (red) and Ge (green).

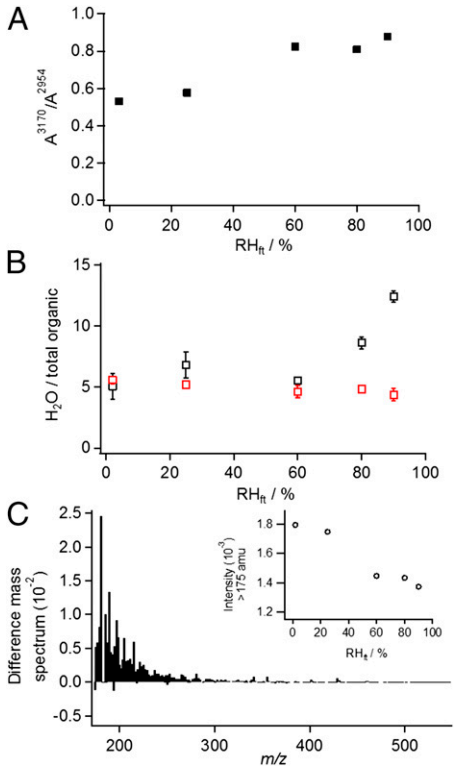

Fig. 5. (*A*) Ratio of peaks resulting from –COOH (3,170 cm^{-1}) and –C-H (2,954 cm^{-1}) as a function of RH_{ft} for impacted SOA. (*B*) Water fragment content (H_2O^+) normalized to the total organic mass as a function of RH_{ft} from AMS measurements directly from the flow tube (black) or through diffusion driers (red). (*C*) Difference aerosol mass spectrum of SOA at <3% RH_{ft} minus that at 90% RH_{ft} (dried). (*Inset*) The sum of intensities >175 atomic mass unit as a function of RH_{ft}. Aerosol mass spectra were normalized to the total mass loading of the <3% RH_{ft} spectrum before subtraction.

shape of the size distribution of the dry SOA did not change significantly on dilution in dry or humid air (*SI Appendix*, Fig. S8). Fig. 4 *A–D* shows the impaction patterns for these dry-wet experiments. The photographs (Fig. 4, *First row*) clearly show that even at the highest RH_{entry} of 85% (RH_I = 68–84%), there is a great deal of particle bounce, consistent with solid (or semi-solid) particles. The SEM images and elemental maps show that as the RH is increased, the spots between the midlines and the presence of carbon along the centerline become somewhat more obvious. However, bounce still dominates so that the relative amounts collected along the centerline are not sufficient to shield the underlying Ge, as was the case for SOA formed in the presence of water vapor (Fig. 3).

Although it was not possible to directly measure the viscosity of the particles as a function of the RH at which they were formed, some limits can be inferred from the extent to which the material collected in the centerline spreads under the high airflow in the impactor. As described in detail in *SI Appendix, Viscosity of SOA at high RH_{ft}* (*SI Appendix*, Figs. S9 and S10), sucrose particles at various RH covering a range of viscosities from liquid to solid (56) were used for comparison. The liquid sucrose (maximum viscosity ∼7 Pa·s at the minimum impactor RH of 71%) undergoes significant spread on the crystal in the direction of the airflow, whereas the material along the centerline at minimum impactor RH of 49% corresponding to a maximum of 8.9×10^3 Pa·s clearly undergoes little spread (but a significant amount of bounce as well). SOA formed at the highest RH studied (87%) falls between the two extremes, with the images suggesting it is closer to the higher-viscosity sucrose. The SEM images (Fig. 3*D*) show "fingers" extending out in the direction of the airflow, suggesting some flow capacity of the SOA or some dissolution in the water present on the substrate at the highest RH. This effect is not present in any other cases. We emphasize that this comparison is intended to simply bracket the likely range of the SOA viscosity, and not be a quantitative measurement. This does, however, highlight the importance of developing accurate methods of measuring viscosities of SOA as a function of formation RH, as well as postformation RH. Absolute viscosity measurements for SOA are currently in their infancy, but recent progress is promising (22, 56).

In short, SOA formed dry and then humidified continues to bounce at the highest RH that was experimentally accessible, whereas much greater amounts of hit and stick (indicative of a lower viscosity) along the centerline are observed for SOA formed in the presence of high concentrations of water vapor. This clearly illustrates that increasing RH is not simply changing the nature of the impaction process but the phase/viscosity of the SOA must be changing as well.

Variation of Composition with Formation RH. A significant advantage of the impactor is that IR spectra can be obtained from the same sample as the impaction patterns. ATR-Fourier transform IR (ATR-FTIR) spectra were recorded immediately after impaction, with the contribution of gas phase and adsorbed water subtracted out (*SI Appendix*, Fig. S11). The spectra were very similar to those reported in the literature for this system (57–59). Quantitative treatment of the spectra in *SI Appendix*, Fig. S11, using the peaks at 3,170 cm^{-1} resulting from carboxylic acids, and 2,954 cm^{-1} resulting from C–H stretches, shows that –COOH groups increase by ∼35% relative to C–H over the range of RH_{ft} from 0–87% (Fig. 5*A*). The presence of carboxylic acids was confirmed by measuring the conversion of carboxylic acid to carboxylate groups by reaction with gas-phase ammonia (*SI Appendix, IR Spectra*; *SI Appendix*, Fig. S12).

To quantify water associated with the SOA, AMS was applied to SOA either sampled directly from the flow tube or passed through two diffusion driers ahead of the AMS (*SI Appendix, Aerosol Mass Spectrometry Measurements*). Fig. 5*B* shows the ratio of the H_2O^+ fragment to the total organic mass as a function of RH for both conditions. At RH up to 60%, the ratio is approximately constant both with and without drying of the particles [the nonzero signal, at low RH reflects H_2O fragments from the decomposition of oxygen-containing organic ions (60) and potentially small amounts of trapped water that are not removed by the driers]. However, at 80% and 90% RH, there is a significant increase in the water content for the SOA sampled directly (at RH_{ft}) versus dried, indicating the presence of water in the particles that can be removed during the ∼75-s residence time in the driers. Because further water evaporation occurs in the lens of the AMS (61), the water content of the particles determined using Fig. 5*B* is likely an underestimate.

Viscosity is expected to be in part related to the average molar mass of the constituents in the particles, which can be probed using AMS. Even under the relatively harsh analysis conditions

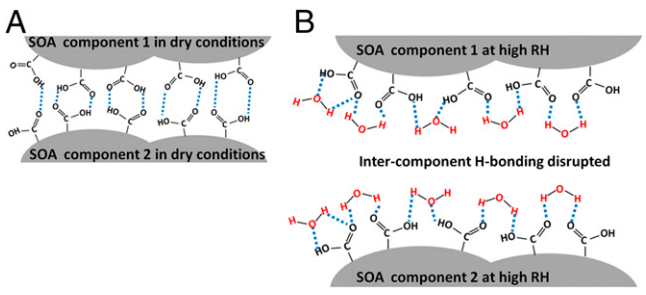

Fig. 6. Illustration of the intercomponent hydrogen bonding responsible for the high viscosity at low RH (*A*), and how this is disrupted in the presence of water (*B*). "SOA component" could be any organic moiety from a semi-volatile organic compound to a cluster of organics to another particle.

(vaporizer temperature at 600 °C and a 70 eV electron impact ionization), peaks up to m/z ~450 are still observed in the mass spectrum under dry conditions. Such high mass peaks are indicative of the presence of oligomers, which are known to be formed in this reaction (62–64). Fig. 5*C* shows a difference spectrum for SOA formed at RH_{ft} <3% minus that at 90% after normalizing to total mass. There is clearly more high-molecular-weight material (m/z > 175) in the dry SOA than the wet SOA, indicating that oligomers are more prevalent in the dry case. A similar analysis at the intermediate RH_{ft} shows a trend of fewer high mass peaks, and therefore oligomers, as RH_{ft} increases (Fig. 5*C*, *Inset*).

Integrating Phase, Viscosity, and Composition of Laboratory-Generated SOA. An interpretation that is consistent with all of the data is the following: Nucleation occurs via the formation of high-molecular-weight oligomers from the reactions of the Criegee intermediate (63, 65–69), and then the particles grow through the condensation of lower-molecular-weight products. Reports of the effects of water vapor on SOA composition from α-pinene ozonolysis are somewhat inconsistent (70–74). However, it is expected on a mechanistic basis that as the RH increases, the Criegee intermediate will be increasingly intercepted by water, generating smaller acids and hydroxyhydroperoxides that can decompose to aldehydes/ketones and H_2O_2 (67, 75). This is consistent with the correlation of RH_{ft} with –COOH (Fig. 5*A*) and the decrease in higher-molecular-mass species by AMS (Fig. 5*C*).

The relationship between viscosity and composition has been explored in a number of studies for both polymeric materials and single organic compounds. In the case of polymers, viscosity increases with the average molar mass; in addition, branched chain polymers have higher viscosity than the corresponding linear chains (76). SOA contains polymeric-type components (oligomers), many of which will be nonlinear. A decrease in higher-molecular-weight species with increasing RH would be expected to lead to a decrease in viscosity, as indicated by the experimental data.

A second factor is that models probing the relationship between viscosity and molecular structure of individual organic compounds show that hydrogen bonding is the most important factor in determining viscosity (77, 78). SOA contains many groups that strongly hydrogen bond, such as –COOH, –OH, –OOH, –CHO, and –C(O)–. Hydrogen bonding between organic components in the particles, including the oligomeric chains, will be a major contributor to the high viscosity of the SOA at low RH_{ft} (Fig. 6*A*). Although –COOH increases with RH_{ft}, the water available during the reaction increases much more and can also hydrogen bond with these SOA functional groups. As shown in previous studies (21), the growth of SOA in this system is best described by a condensation-type mechanism in which molecules irreversibly add to the growing particle. As products with hydrogen-bonding capable functional groups are added to the particle surface, the formation of hydrogen bonds with water that is readily available in the gas phase, rather than to other organics, will become more important (Fig. 6*B*). This effectively "caps off" the formation of strongly hydrogen-bonded aggregates of organics and/or oligomers, leaving smaller components that have water attached to the SOA oxidized functional groups. The chains and molecules can then move independently, resulting in reduced viscosity. Water incorporated into the particles in this manner should be relatively easily removed in the diffusion driers (Fig. 5*B*) because it is not covalently bound, and the particles are sufficiently small that the characteristic times for diffusion (31) in the particle bulk are small compared with the residence time in the driers. A similar effect has been observed with aqueous sucrose particles (56), where the viscosity diverges from that predicted by orders of magnitude as the mole fraction of sucrose increases because of the formation of intermolecularly bonded sucrose networks.

Renbaum-Wolff and coworkers (22) recently reported viscosity measurements for supermicron particles of the water-soluble fraction of SOA that was subsequently humidified to various RH. Our dry-wet experiments are the most comparable to that work, although in our experiments, the SOA was directly probed without collection and extraction. In the present experiments, particle bounce characteristic of solid or semisolid particles occurred at all RH (Fig. 4, *First row*), and the viscosity does not appear to change significantly with increasing RH, at least at the mixing times used here (*SI Appendix*, *Effect of Varying RH_f on Impaction Patterns*). This is consistent with what might be expected according to the known limited water uptake behavior of SOA (79, 80). The observation of Renbaum-Wolff and coworkers (22) that viscosity declined with secondary exposure to water vapor from values consistent with semisolids (10^{12}–10^2 Pa·s) for 40–80% RH to ~10 Pa·s between 80% and 90% RH may reflect the increased hydrophilicity of their water-extracted SOA. Our results for SOA formed in the presence of water show that there is an apparent reduction in viscosity at the highest RH studied, but it is far from a low-viscosity liquid. In summary, the phase and viscosity of SOA are clearly affected by changes in RH both during SOA formation and after.

Methods and Materials

SOA was generated at various RH from O_3 (650 ppb) and α-pinene (800 ppb) in a large-volume flow tube (21, 52). SOA was sampled after a reaction time of ~30 min at 30 L·min^{-1}, using a custom-built ATR impactor with a d_{50} = 240 ± 12 nm. Total mass concentrations were ~1,000 μg·m^{-3}. In the dry-wet experiments, SOA was generated at <3% RH and then diluted in humid air for a mixing time of ~76 ms. The patterns formed by aerosol particles impacting a Ge ATR crystal were captured by digital photography and SEM; their composition was probed by ATR-FTIR and time-of-flight AMS (Aerodyne). Size distributions were recorded using a scanning mobility particle sizer and an aerodynamic particle sizer. In a separate set of experiments, the amount of dry sucrose particles exiting the impactor was used to estimate, by difference, the amount of material collected on the substrate. This showed that 60–80% of the particles were collected, which represents a lower limit for the lower-density SOA. Additional experiments were carried out using atomized standards (Na_2SO_4, caffeine and CML spheres). Details of all experiments are found in the *SI Appendix*.

ACKNOWLEDGMENTS. We thank Sergey Nizkorodov for helpful discussions; Dr. Jian-Guo Zheng at the Laboratory for Electron and X-ray Instrumentation at the University of California, Irvine; Lee Moritz and Ron Hulme for technical assistance; James N. Pitts, Jr., for comments on the manuscript; and the anonymous reviewers for helpful suggestions. The authors are grateful to the National Science Foundation (Grants 1207112 and 0909227) and the Department of Energy (Grant ER65208) for funding.

1. Pope CA, 3rd, Dockery DW (2006) Health effects of fine particulate air pollution: Lines that connect. *J Air Waste Manag Assoc* 56(6):709–742.
2. Finlayson-Pitts BJ, Pitts JN, Jr. (2000) *Chemistry of the upper and lower atmosphere - theory, experiments, and applications* (Academic Press, San Diego).
3. Seinfeld JH, Pandis SN (2006) *Atmospheric chemistry and physics: From air pollution to climate change* (Wiley-Interscience, New York).
4. Hinds WC (1999) *Aerosol technology: Properties, behavior and measurement of airborne particles* (John Wiley & Sons Inc., New York).
5. Ramanathan V, Feng Y (2009) Air pollution, greenhouse gases and climate change: Global and regional perspectives. *Atmos Environ* 43:37–50.
6. Pöschl U (2005) Atmospheric aerosols: Composition, transformation, climate and health effects. *Angew Chem Int Ed Engl* 44(46):7520–7540.
7. Intergovernmental Panel on Climate Change (2013) Climate Change 2013: The Physical Science Basis: Summary for Policy Makers. Available at http://www.climatechange2013.org/images/report/WG1AR5_SPM_FINAL.pdf. Accessed December 1, 2013.
8. Jimenez JL, et al. (2009) Evolution of organic aerosols in the atmosphere. *Science* 326(5959):1525–1529.
9. Liggio J, et al. (2010) Primary and secondary organic aerosols in urban air masses intercepted at a rural site. *J Geophys Res* 115:10.1029/2010JD014426.
10. Ng NL, et al. (2010) Organic aerosol components observed in northern hemispheric datasets from aerosol mass spectrometry. *Atmos Chem Phys* 10:4625–4641.
11. Carlton AG, et al. (2010) Model representation of secondary organic aerosol in CMAQv4.7. *Environ Sci Technol* 44(22):8553–8560.
12. Shrivastava M, et al. (2011) Modeling organic aerosols in a megacity: Comparison of simple and complex representations of the volatility basis set approach. *Atmos Chem Phys* 11:6639–6662.
13. Foley KM, et al. (2010) Incremental testing of the community multiscale air quality (CMAQ) modeling system version 4.7. *Geosci Model Dev* 3:205–226.
14. Tsimpidi AP, et al. (2010) Evaluation of the volatility basis-set approach for the simulation of organic aerosol formation in the Mexico City metropolitan area. *Atmos Chem Phys* 10:525–546.

15. Fast J, et al. (2009) Evaluating simulated primary anthropogenic and biomass burning organic aerosols during MILAGRO: Implications for assessing treatments of secondary organic aerosols. *Atmos Chem Phys* 9:6191–6215.
16. Dzepina K, et al. (2011) Modeling the multiday evolution and aging of secondary organic aerosol during MILAGRO 2006. *Environ Sci Technol* 45(8):3496–3503.
17. Donahue NM, Robinson AL, Stanier CO, Pandis SN (2006) Coupled partitioning, dilution, and chemical aging of semivolatile organics. *Environ Sci Technol* 40(8): 2635–2643.
18. Pankow J (1994) An absorption model of gas/particle partioning of organic compounds in the atmosphere. *Atmos Environ* 28:185–188.
19. Abramson E, Imre D, Beránek J, Wilson J, Zelenyuk A (2013) Experimental determination of chemical diffusion within secondary organic aerosol particles. *Phys Chem Chem Phys* 15(8):2983–2991.
20. Vaden TD, Imre D, Beránek J, Shrivastava M, Zelenyuk A (2011) Evaporation kinetics and phase of laboratory and ambient secondary organic aerosol. *Proc Natl Acad Sci USA* 108(6):2190–2195.
21. Perraud V, et al. (2012) Nonequilibrium atmospheric secondary organic aerosol formation and growth. *Proc Natl Acad Sci USA* 109(8):2836–2841.
22. Renbaum-Wolff L, et al. (2013) Viscosity of α-pinene secondary organic material and implications for particle growth and reactivity. *Proc Natl Acad Sci USA* 110(20): 8014–8019.
23. Vaden TD, Song C, Zaveri RA, Imre D, Zelenyuk A (2010) Morphology of mixed primary and secondary organic particles and the adsorption of spectator organic gases during aerosol formation. *Proc Natl Acad Sci USA* 107(15):6658–6663.
24. Kuwata M, Martin ST (2012) Phase of atmospheric secondary organic material affects its reactivity. *Proc Natl Acad Sci USA* 109(43):17354–17359.
25. Cappa CD, Wilson KR (2011) Evolution of organic aerosol mass spectra upon heating: Implications for OA phase and partitioning behavior. *Atmos Chem Phys* 11:1895–1911.
26. Virtanen A, et al. (2010) An amorphous solid state of biogenic secondary organic aerosol particles. *Nature* 467(7317):824–827.
27. Virtanen A, et al. (2011) Bounce behavior of freshly nucleated biogenic secondary organic aerosol particles. *Atmos Chem Phys* 11:8759–8766.
28. Saukko E, et al. (2012) Humidity-dependent phase state of SOA particles from biogenic and anthropogenic precursors. *Atmos Chem Phys* 12:7517–7529.
29. Saukko E, Kuuluvainen H, Virtanen A (2012) A method to resolve the phase state of aerosol particles. *Atmos Meas Tech* 5:259–265.
30. Koop T, Bookhold J, Shiraiwa M, Pöschl U (2011) Glass transition and phase state of organic compounds: Dependency on molecular properties and implications for secondary organic aerosols in the atmosphere. *Phys Chem Chem Phys* 13(43):19238–19255.
31. Shiraiwa M, Ammann M, Koop T, Pöschl U (2011) Gas uptake and chemical aging of semisolid organic aerosol particles. *Proc Natl Acad Sci USA* 108(27):11003–11008.
32. Zobrist B, Marcolli C, Pedernera DA, Koop T (2008) Do atmospheric aerosols form glasses? *Atmos Chem Phys* 8:5221–5244.
33. Winkler P (1974) Relative humidity and the adhesion of atmospheric particles to the plates of impactors. *J Aerosol Sci* 5:235–240.
34. Riipinen I, et al. (2011) Organic condensation: A vital link connecting aerosol formation to cloud condensation nuclei (CCN) concentrations. *Atmos Chem Phys* 11: 3865–3878.
35. Shrivastava M, et al. (2013) Implications of low volatility SOA and gas-phase fragmentation reactions on SOA loadings and their spatial and temporal evolution in the atmosphere. *J Geophys Res* 118:3328–3342.
36. Kidd C, Perraud V, Finlayson-Pitts BJ (2014) Surfactant-free latex spheres for size calibration of mobility particle sizers in atmospheric aerosol applications. *Atmos Environ* 82:56–59.
37. Chang MC, Kim S, Sioutas C (1999) Experimental studies on particle impaction and bounce: Effects of substrate design and material. *Atmos Environ* 33:2313–2322.
38. Rao AK, Whitby KT (1978) Non-ideal collection characteristics of inertial impactors—I. Single-stage impactors and solid particles. *J Aerosol Sci* 9:77–86.
39. Turner JR, Hering SV (1987) Greased and oiled substrates as bounce-free impaction surfaces. *J Aerosol Sci* 18:215–224.
40. Tsai CJ, Cheng YH (1995) Solid particle collection characteristics on impaction surfaces of different designs. *Aerosol Sci Technol* 23:96–106.
41. Wang HC, John W (1987) Comparative bounce properties of particle materials. *Aerosol Sci Technol* 7:285–299.
42. Matthew BM, Middlebrook AM, Onasch TB (2008) Collection efficiencies in an aerodyne aerosol mass spectrometer as a function of particle phase for laboratory generated aerosols. *Aerosol Sci Technol* 42:884–898.
43. Middlebrook AM, Bahreini R, Jimenez JL, Canagaratna MR (2011) Evaluation of composition-dependent collection efficiencies for the aerodyne aerosol mass spectrometer using field data. *Aerosol Sci Technol* 46:258–271.
44. Kuuluvainen H, Arffman A, Saukko E, Virtanen A, Keskinen J (2013) A new method for characterizing the bounce and charge transfer properties of nanoparticles. *J Aerosol Sci* 55:104–115.
45. Rocklage JM, Marple VA, Olson BA (2013) Study of secondary deposits in multiple round nozzle impactors. *Aerosol Sci Technol* 47:1144–1151.
46. Paw UKT, Braaten DA (1995) New perspectives on rebound and reentrainment processess. *Aerosol Sci Technol* 23:72–79.
47. Dahneke B (1971) Capture of aerosol particles by surfaces. *J Colloid Interface Sci* 37:342–352.
48. Esmen NA, Ziegler P, Whitfield R (1978) The adhesion of particles upon impaction. *J Aerosol Sci* 9:547–556.
49. Tsai CJ, Pui DYH, Liu BYH (1991) Elastic flattening and particle adhesion. *Aerosol Sci Technol* 15:239–255.
50. Rogers LN, Reed J (1984) The adhesion of particles undergoing an elastic plastic impact with a surface. *J Phys D Appl Phys* 17:677–689.
51. Sethi V, John W (1993) Particle impaction patterns from a circular jet. *Aerosol Sci Technol* 18:1–10.
52. Ezell MJ, et al. (2010) A new aerosol flow system for photochemical and thermal studies of tropospheric aerosols. *Aerosol Sci Technol* 44:329–338.
53. Stein SW, Turpin BJ, Cai XP, Huang CPF, McMurry PH (1994) Measurement of relative humidity-dependent bounce and density for atmospheric particles using the DMA-impactor technique. *Atmos Environ* 28:1739–1746.
54. Chen S-C, Tsai C-J, Chen H-D, Huang C-Y, Roam G-D (2011) The influence of relative humidity on nanoparticle concentration and particle mass distribution measurements by the MOUDI. *Aerosol Sci Technol* 45:596–603.
55. Bateman AP, Belassein H, Martin ST (2014) Impactor apparatus for the study of particle rebound: Relative humidity and capillary forces. *Aerosol Sci Tech* 42–52.
56. Power RM, Simpson SH, Reid JP, Hudson AJ (2013) The transition from liquid to solid-like behaviour in ultrahigh viscosity aerosol particles. *Chemical Science* 4:2597–2604.
57. Hung H-M, Chen Y-Q, Martin ST (2013) Reactive aging of films of secondary organic material studied by infrared spectroscopy. *J Phys Chem A* 117(1):108–116.
58. Bruns EA, Perraud V, Greaves J, Finlayson-Pitts BJ (2010) Atmospheric solids analysis probe mass spectrometry: A new approach for airborne particle analysis. *Anal Chem* 82(14):5922–5927.
59. Sax M, Zenobi R, Baltensperger U, Kalberer M (2005) Time resolved infrared spectroscopic analysis of aerosol formed by photo-oxidation of 1,3,5-trimethylbenzene and alpha-pinene. *Aerosol Sci Technol* 39:822–830.
60. Aiken AC, et al. (2008) O/C and OM/OC ratios of primary, secondary, and ambient organic aerosols with high-resolution time-of-flight aerosol mass spectrometry. *Environ Sci Technol* 42(12):4478–4485.
61. Zelenyuk A, Imre D, Cuadra-Rodriguez LA (2006) Evaporation of water from particles in the aerodynamic lens inlet: An experimental study. *Anal Chem* 78(19):6942–6947.
62. Reinhardt A, et al. (2007) Ultrahigh mass resolution and accurate mass measurements as a tool to characterize oligomers in secondary organic aerosols. *Anal Chem* 79(11): 4074–4082.
63. Hall WAI, 4th, Johnston MV (2012) Oligomer formation pathways in secondary organic aerosol from MS and MS/MS measurements with high mass accuracy and resolving power. *J Am Soc Mass Spectrom* 23(6):1097–1108.
64. Kalberer M, et al. (2004) Identification of polymers as major components of atmospheric organic aerosols. *Science* 303(5664):1659–1662.
65. Zhao J, Ortega J, Chen M, McMurry PH, Smith JN (2013) Dependence of particle nucleation and growth on high-molecular-weight gas-phase products during ozonolysis of α-pinene. *Atmos Chem Phys* 13:7631–7644.
66. Sadezky A, et al. (2008) Oligomer formation during gas-phase ozonolysis of small alkenes and enol ethers: New evidence for the central role of the Criegee intermediate as oligomer chain unit. *Atmos Chem Phys* 8:2667–2669.
67. Johnson D, Marston G (2008) The gas-phase ozonolysis of unsaturated volatile organic compounds in the troposphere. *Chem Soc Rev* 37(4):699–716.
68. Lee CT, Kamens RM (2005) Particle nucleation from the reaction of α−pinene and O_3. *Atmos Environ* 39:6822–6832.
69. Vereecken L, Harder H, Novelli A (2012) The reaction of Criegee intermediates with NO, RO_2, and SO_2, and their fate in the atmosphere. *Phys Chem Chem Phys* 14(42): 14682–14695.
70. Warscheid B, Hoffmann T (2001) On-line measurements of α-pinene ozonolysis products using an atmospheric pressure chemical ionization ion-trap mass spectrometer. *Atmos Environ* 35:2927–2940.
71. Fick J, Pommer L, Nilsson C, Andersson B (2003) Effect of OH radicals, relative humidity, and time on the composition of the products formed in the ozonolysis of alpha-pinene. *Atmos Environ* 37:4087–4096.
72. Ma Y, et al. (2007) Organic acid formation in the gas-phase ozonolysis of α-pinene. *Phys Chem Chem Phys* 9(37):5084–5087.
73. Christofferson TS, et al. (1998) Cis-pinic acid, a possible precursor for organic aerosol formation from ozonolysis of α-pinene. *Atmos Environ* 32:1657–1661.
74. Winterhalter R, Van Dingenen R, Larsen BR, Jensen NR, Hjorth J (2003) LC-MS analysis of aerosol particles from the oxidation of α-pinene by ozone and OH radicals. *Atmos Chem Phys Discuss* 3:1–39.
75. Ma Y, Willcox TR, Russell AT, Marston G (2007) Pinic and pinonic acid formation in the reaction of ozone with α-pinene. *Chem Commun (Camb)* (13):1328–1330.
76. Muenstedt H (2011) Rheological properties and molecular structure of polymer melts. *Soft Matter* 7:2273–2283.
77. Lučić B, et al. (2002) Correlation of liquid viscosity with molecular structure for organic compounds using different variable selection methods. *ARKIVOC* 4:45–59.
78. Gharagheizi F, Mirkhani SA, Keshavarz MH, Farahani N, Tumba K (2013) A molecular-based model for prediction of liquid viscosity of pure organic compounds: A quantitative structure property relationship (QSPR) approach. *J Taiwan Inst Chem E* 44: 359–364.
79. Varutbangkul V, et al. (2006) Hygroscopicity of secondary organic aerosols formed by oxidation of cycloalkenes, monoterpenes, sesquiterpenes, and related compounds. *Atmos Chem Phys* 6:2367–2388.
80. Cocker DR, Clegg SL, Flagan RC, Seinfeld JH (2001) The effect of water on gas-particle partitioning of secondary organic aerosol. Part I: Alpha-pinene/ozone system. *Atmos Environ* 35:6049–6072.